Large-deformation finite element analysis of pipe penetration and large-amplitude lateral displacement

Dong Wang, David J. White, and Mark F. Randolph

Abstract: Seabed pipelines must be designed to accommodate thermal expansion — which is commonly achieved through controlled lateral buckling — and to resist damage from submarine slides. In both cases, the pipe moves laterally by a significant distance and the overall pipeline response is strongly influenced by the lateral pipe–soil resistance. Here, the process of pipe penetration and lateral displacement is investigated using a large-deformation finite element method, with a softening rate–dependent soil model being incorporated. The calculated soil flow mechanisms, pipe resistances, and trajectories agree well with plasticity solutions and centrifuge test data. It was found that the lateral resistance is strongly influenced by soil heave during penetration and the berm formed ahead of the pipe during lateral displacement. For "light" pipes, the pipe rises to the soil surface and the soil failure mechanism involves sliding at the base of the berm. In contrast, "heavy" pipes dive downwards and a deep shearing zone is mobilized, expanding with continuing lateral movement. The different responses are reconciled by defining an "effective embedment" that includes the effect of the soil berm or wall ahead of the pipe. The relationship between normalized lateral resistance and effective embedment is well fitted using a power law.

Key words: pipeline, clay, finite element method, buckling, penetration.

Résumé : Les tuyaux placés au fond de la mer doivent être conçus de manière à contenir l'expansion thermique — ce qui est normalement accompli par flambement latéral contrôlé — et à résister aux dommages causés par les glissements sous-marins. Dans les deux cas, le tuyau se déplace latéralement sur une distance significative, et le comportement global du tuyau est fortement influencé par la résistance latérale entre le tuyau et le sol. Dans cet article, le processus de pénétration du tuyau et de déplacement latéral est évalué à l'aide d'une méthode par éléments finis pour les grands déplacements, à laquelle un modèle de sol avec l'adoucissement des déformations dépendant d'un taux est ajouté. Les mécanismes d'écoulement, les résistances des tuyaux et les trajectoires calculés correspondent bien avec les solutions de la théorie de la plasticité et les données des essais à la centrifuge. Il a été déterminé que la résistance latérale est fortement influencée par le soulèvement du sol durant la pénétration et aussi par la berme formée au devant du tuyau durant le déplacement latéral. Dans le cas de tuyaux « légers », le tuyau monte à la surface du sol et un glissement à la base de la berme est impliqué dans le mécanisme de rupture du sol. À l'opposé, les tuyaux « lourds » se déplacent vers le bas et une zone de cisaillement profonde est mobilisée et s'étend à mesure que le mouvement latéral s'avance. Ces comportements différents sont combinés dans le paramètre « enfouissement effectif » qui inclus l'effet de la berme ou du mur en avant du tuyau. La relation entre la résistance latérale normalisée et l'enfouissement effectif est bien représentée par une loi de puissance.

Mots-clés : tuyau, argile, méthode d'éléments finis, flambement, pénétration.

[Traduit par la Rédaction]

Introduction

Seabed pipelines are an increasingly significant component of offshore hydrocarbon developments. As exploration moves into deeper waters, more distant from shore, the design and construction of the seabed pipelines that connect the facility to shore represent a larger proportion of the capital expenditure of the project. In areas where overtrawling is not a hazard, pipelines are generally laid untrenched on the seabed but embed shallowly due to self-weight, additional loads, and dynamic motions imposed during the laying process. The varying temperature and pressure within the pipeline during operation and shutdown cycles lead to thermal expansion, which may be accommodated by controlled lateral buckling (Bruton et al. 2008). Design of on-bottom pipelines with regard to lateral buckling, or other external interaction such as submarine slides, requires assessment of the pipe–soil interaction forces that result from lateral motion.

Geotechnical design procedures for pipelines and risers are relatively undeveloped compared with those for foundations such as footings and piles. Unlike conventional foundations, pipelines and risers are often designed to move significant distances in operation. A foundation or pile is generally designed to deflect by less than a few percent of the diameter. In contrast, the crown of a lateral buckle may

Received 11 September 2008. Accepted 18 December 2009. Published on the NRC Research Press Web site at cgj.nrc.ca on 16 July 2010.

D. Wang,[1] D.J. White, and M.F. Randolph. Centre for Offshore Foundation Systems, The University of Western Australia, 35 Stirling Highway, Crawley, WA6009, Australia.

[1]Corresponding author (e-mail: wang@civil.uwa.edu.au).

move a distance of more than 10 pipe diameters across the seabed. To predict the formation of lateral buckles along the partially embedded pipeline, the lateral soil resistance at different combinations of vertical load and pipeline embedment must be estimated accurately in the pipeline design. The pipeline response within a lateral buckle depends on the magnitude and shape of the large-amplitude load–displacement response. A steady rise in resistance as the pipe displaces further will tend to spread the buckle longitudinally, whereas a constant or softening response leads to increased feed-in of pipe into the buckle. These mechanisms have a significant influence on the bending moment within the pipeline (Konuk and Yu 2007; Bruton et al. 2008).

To design a pipeline to resist submarine slide impact, the large-amplitude lateral load–displacement response of the section of pipeline that lies outside the slide zone, providing passive restraint, must be assessed. Analyses show that the pipe may displace several diameters laterally in a typical design scenario (Swanson and Jones 1982). It is necessary to assess the available lateral resistance over this large movement.

The geometry and nomenclature of a shallow-embedded pipe subjected to lateral movement is illustrated in Fig. 1. The lateral resistance that the pipeline has to overcome during buckle initiation or during a slide impact depends strongly on the pipe embedment, soil strength profile, pipe–soil contact properties, and overpenetration ratio. This ratio is defined as $R = V_{max}/V_{op}$, where V_{max} is the vertical load that is required for further vertical penetration at the current embedment (in the absence of any horizontal load) and V_{op} is the operating load during lateral movement of the pipe. The overpenetration ratio is usually in the range of 1–10.

To assess the ultimate resistance of a pipeline under combinations of vertical and horizontal loading, families of failure envelopes have been proposed using the upper bound plasticity theorem (Cheuk et al. 2008; Randolph and White 2008*a*) and small-strain finite element (FE) method (Aubeny et al. 2005; Merifield et al. 2008*a*, 2008*b*). These failure envelopes have been fitted by simple equations to provide a more practical basis to assess the stability of pipelines (Merifield et al. 2008*a*).

These previous studies have two significant limitations. Firstly, the theoretical studies are concerned only with the lateral response for small pipe movements. The limit plasticity solutions do not consider changes in geometry and therefore provide no information on the large-amplitude behaviour. Also, the pipe is usually assumed to be wished-in-place, so the vertical penetration process and the resulting heave and remoulding of the surrounding soil is neglected, although Merifield et al. (2009) have quantified the influence of heave for purely vertical or purely horizontal loading.

The wished-in-place assumption leads to an underestimation of the vertical penetration resistance and also the horizontal breakout load at a given embedment. The heaved soil leads to pipe–soil contact over more of the pipe perimeter than for a wished-in-place pipe, which increases the resistance to both axial and lateral movement. Also, during large-amplitude lateral movement, the laterally sweeping pipe pushes ahead a soil berm that includes the soil heave from the initial penetration process, increasing the soil berm size as the lateral movement increases.

Fig. 1. Problem definition: pipe–soil interaction. *D*, pipeline diameter; *H*, mobilized lateral resistance; *V*, vertical load per unit length; *w*, embedment; *u*, pipe lateral displacement; *z*, soil depth.

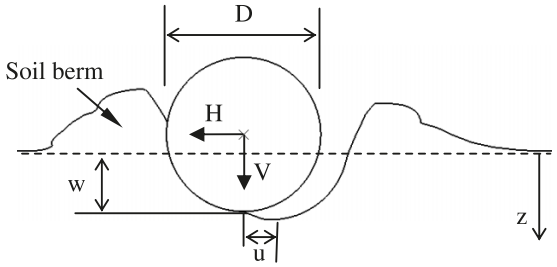

The existence of the soil berm is analogous to an additional degree of embedment relative to the original soil surface. However, the effect of the berm on the lateral resistance during large-amplitude motion is not well understood. Centrifuge tests conducted recently at The University of Western Australia incorporated particle image velocimetry (PIV) and close-range photogrammetry techniques (White et al. 2003) to provide details of the soil flow mechanisms during large-amplitude lateral displacement of a pipeline partially embedded on soft clay (Dingle et al. 2008).

The purpose of this paper is to investigate the full process of undrained penetration and large-amplitude lateral displacement for pipelines embedded in soft clay to quantify the large-amplitude load–displacement response. A two-dimensional large deformation finite element (LDFE) method is adopted, making use of the "remeshing and interpolation technique with small strain" (RITSS; Hu and Randolph 1998). A soil constitutive model considering strain-softening and strain-rate dependence is incorporated in the LDFE simulations. Results from the numerical analyses are compared with those from centrifuge tests of pipe–soil interaction in kaolin clay (Dingle et al. 2008) and existing upper bound solutions (Randolph and White 2008*a*). The large-amplitude lateral behaviour of both "heavy" and "light" pipelines is explored and the effect of the soil berm on the lateral resistance is further discussed. The work here builds on the previous LDFE study by Konuk and Yu (2007), using a rather simpler soil model reflecting the familiar concept of undrained shear strength and considering the effect of surface heave during initial penetration on the subsequent lateral motion.

Procedure of large deformation analysis

The vertical penetration and lateral response of a pipeline is a typical large-deformation problem, associated with large strains and changing geometry. Conventional small-strain FE methods are unable to mimic these processes because the soil elements in the vicinity of the pipeline are grossly distorted. The RITSS avoids mesh distortion by dividing the displacement of the pipeline into a series of incremental steps. In each increment, the displacement must be sufficiently small for the small-strain calculation to be performed. After that, the deformed geometry is generated and remeshed, as well as the field variables being mapped from the old mesh to the new mesh, for the calculation of the next increment. The field variables comprise the stresses, strains,

Fig. 2. Procedure of ABAQUS-based large deformation finite element analysis: (*a*) overall scheme; (*b*) implementation in ABAQUS.

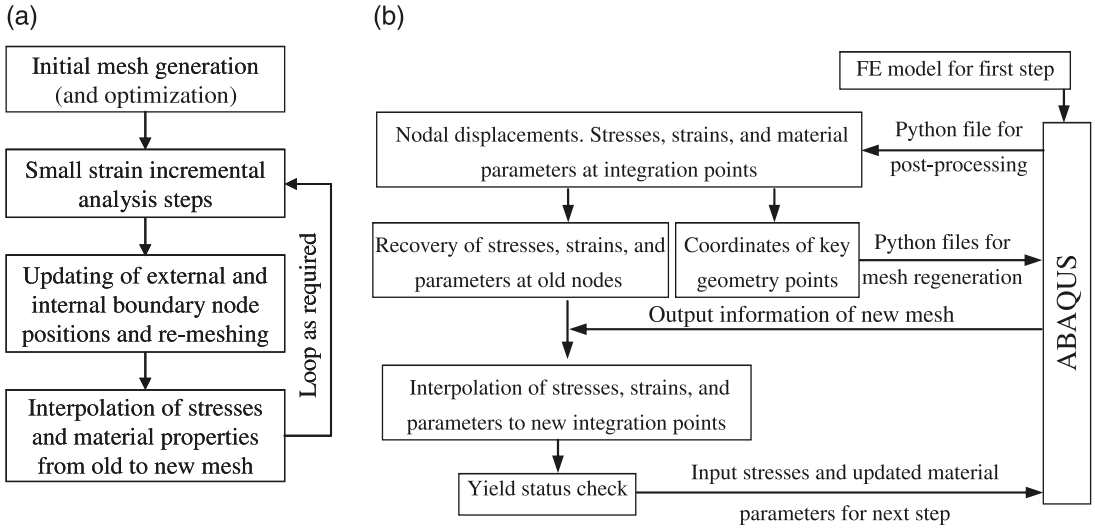

and material properties at the old integration points. The RITSS is essentially an Arbitrary Lagrangian Eulerian method, extended by generating a new mesh before each Eulerian step. Lagrangian calculations are undertaken in each increment and the field variables are then "convected" between the old and new meshes (Hu and Randolph 1998; Randolph et al. 2008). The remeshing is performed within the *deformed* extent of the mesh, allowing the extent of the boundaries to change — for example, through heave of the ground surface.

An advantage of the RITSS is that the remeshing and interpolation algorithm can be coupled with any standard FE program. Previous applications of the RITSS in geomechanics were mainly built around the AFENA (Carter and Balaam 1995) and ABAQUS (HKS 2006) FE codes (Hu and Randolph 1998; Zhou and Randolph 2007; Wang et al. 2006, 2010). In this work, ABAQUS is called by a master program (written in Fortran) to mesh and perform a small-strain calculation in each increment. Python, which is the script language built into ABAQUS, has been used both to write code that extracts the field variables from the result files and to control the mesh density during mesh regeneration. With these techniques the LDFE analysis can be implemented continuously and automatically without requiring any intervention from the user. The small-strain FE calculation in each increment is based on Lagrangian formulae, with the strains and stresses computed using Green strain tensors and Cauchy stress tensors, respectively. The Green–Cauchy deformation tensors are rotation-independent, but the rotations within each small-strain step are negligibly small. Any out-of-balance forces resulting from geometry changes (including rigid body rotation) or minor errors in interpolation during the Eulerian stage are carried forward into the following increment, obviating the need to adopt a large-strain formulation in the Lagrangian calculations. The accuracy of the RITSS method has been verified through its applications to analysis of penetrometers, shallow footings, and plate anchors, with the results being benchmarked against analytical solutions (Randolph et al. 2008).

The pipeline–soil interaction is treated as a plane strain problem, with the soil being meshed using quadratic triangular elements. As the pipe in practice is much stiffer than the soil and the stress distributions in the pipe are not of concern, the pipe was modelled as a discrete rigid body. A strategy termed "superconvergent patch recovery" (Zienkiewicz and Zhu 1992) is applied to extrapolate soil stresses, strains, and material parameters from the old integration points to the element nodes, followed by interpolation from the old element nodes to new integration points. The recovery and interpolation of the field variables is carried out externally by subroutines written in Fortran. The overall RITSS scheme and its implementation in ABAQUS are shown schematically in Fig. 2, where the sequence of small-strain computing, remeshing, and mapping is repeated until the required vertical or lateral movement of the pipe is reached. Further details of these procedures can be found in Wang et al. (2006, 2010).

Strain rate and strain-softening

In situ tests, such as T-bar or spherical ball penetration, are commonly used to assess the shear strength profile of the seabed. These tests can be used to quantify the strain-softening and rate-dependence of the soil strength, s_u, during undrained shearing. Accurate modelling of large-strain processes, such as pipe penetration and large-displacement lateral breakout, requires inclusion of these effects. The simplest approach is to adjust the basic profile of undrained strength to reflect rate-dependence and strain softening. An empirical expression, which has been widely used in simulations of penetrometer testing, is (Einav and Randolph 2005; Zhou and Randolph 2007)

$$[1] \qquad s_u = \left\{1 + \mu \log\left[\frac{\max\left(|\dot{\gamma}_{max}|, \dot{\gamma}_{ref}\right)}{\dot{\gamma}_{ref}}\right]\right\} \times \left[\delta_{rem} + (1 - \delta_{rem})e^{-3\xi/\xi_{95}}\right] s_{u0}$$

where the first and second bracketed terms represent the effect of strain rate and strain softening, respectively, s_{u0} is the

Fig. 3. Calculated and measured profiles of penetration resistance: (*a*) from LDFE and upper bound plasticity analysis (ideal soil, no softening or rate effects); (*b*) LDFE and centrifuge test ($\gamma' D/s_{um} = 2.26$).

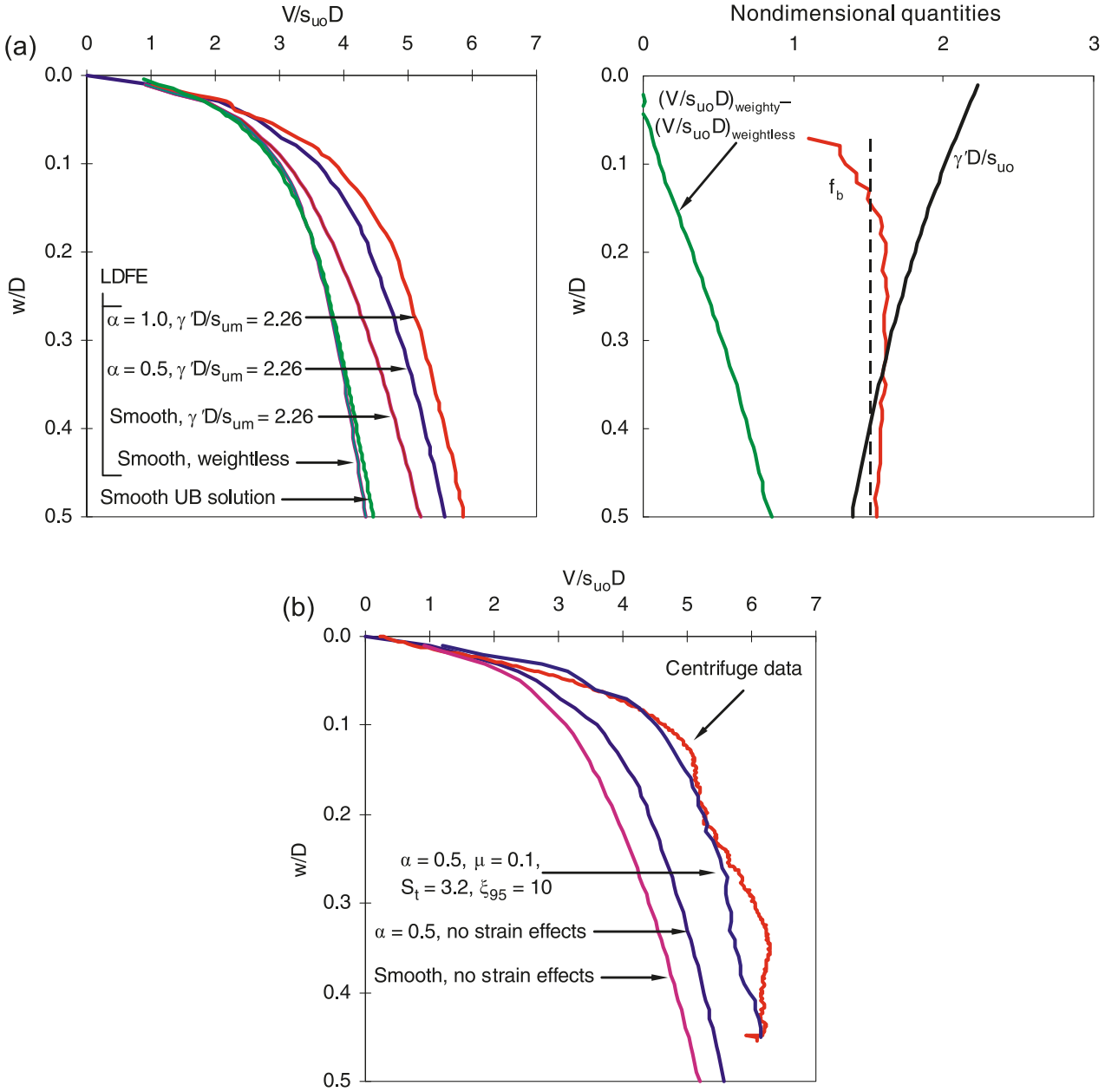

original shear strength at the reference shear strain rate prior to any softening, and the other variables used in this equation are defined in the next two paragraphs. This model provides a value of shear strength for use in the Tresca failure criterion.

In the first bracket of eq. [1], the rate of strength increase per decade, μ, is typically between 0.05 and 0.2, $\dot{\gamma}_{ref}$ is the reference shear strain rate and is usually taken as 3×10^{-6} 1/s ($\sim$1%/h), and $\dot{\gamma}_{max}$ is defined as

$$[2] \qquad \dot{\gamma}_{max} = \frac{\Delta\varepsilon_1 - \Delta\varepsilon_3}{\Delta t}$$

$$[3] \qquad \Delta t = \delta / v_p$$

where $\Delta\varepsilon_1$ and $\Delta\varepsilon_3$ are cumulative major and minor principal strains, δ is the specified incremental displacement in each increment, and v_p is the pipeline penetration rate.

In the second bracket of eq. [1], δ_{rem} is the ratio between the fully remoulded and initial shear strengths, i.e., the inverse of the remoulded sensitivity, S_t; ξ denotes the accumulated absolute plastic shear strain; and ξ_{95} represents the value of ξ at which the soil has undergone 95% of the reduction in strength due to remoulding. Typical values of ξ_{95} estimated from the results of cyclic penetrometer tests are in the range 10$\sim$30 (Zhou and Randolph 2010).

If the constitutive model coupled with the RITSS approach is strain-independent, it is not necessary to map strains from the old mesh to the new mesh, such as in the

Fig. 4. Instantaneous velocity field during penetration (softening rate-dependent strength used in FE). *x*, horizontal coordinate.

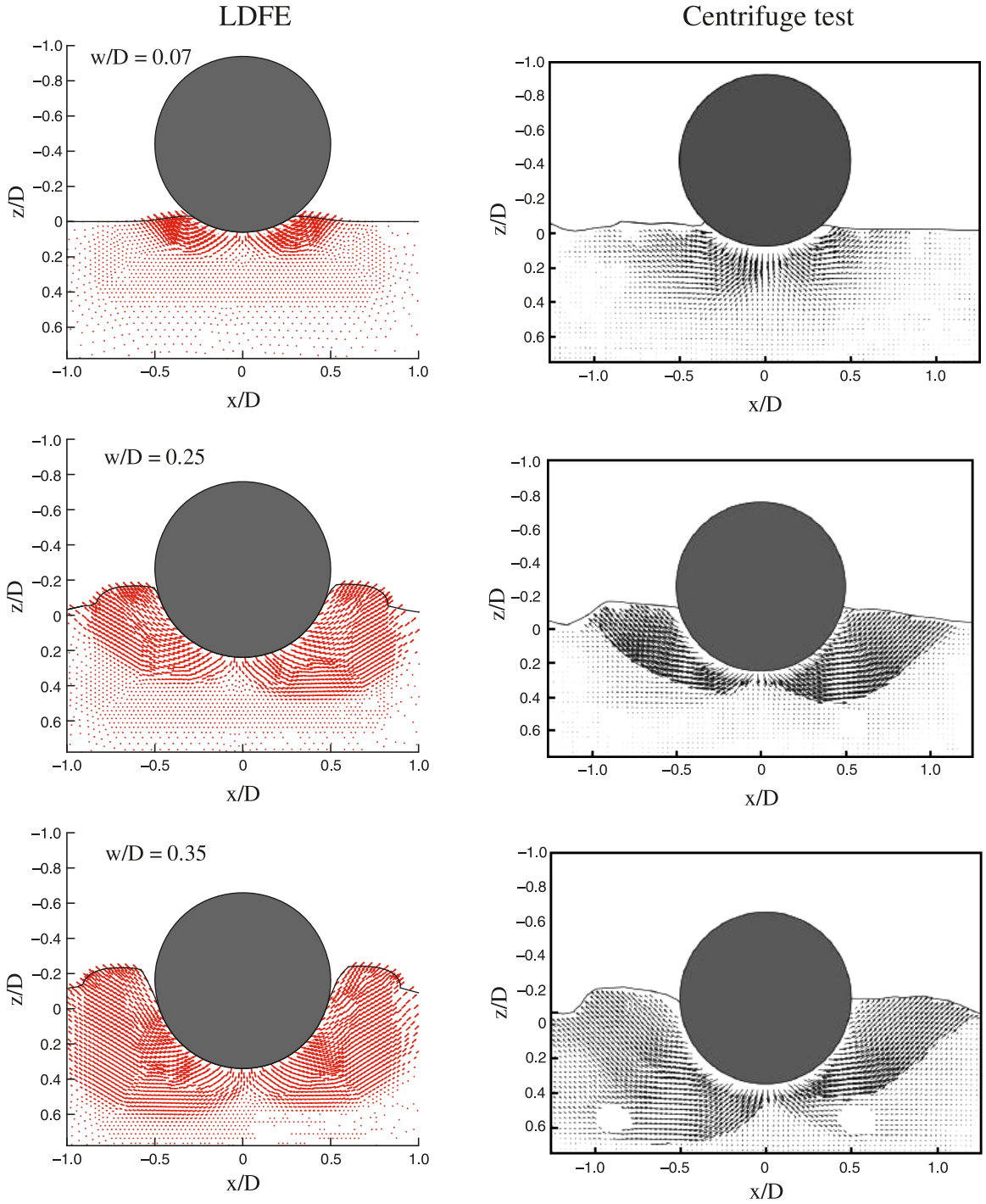

applications described by Zhou and Randolph (2010). In contrast, if eq. [1] is used, the maximum shear strain and plastic shear strain at old integration points have to be recorded and then interpolated onto new integration points to continually update the soil shear strength in the whole region. The updated strength is taken as constant during the small-strain calculations of each increment.

FE results and discussions

Problem definition and parameters

The LDFE approach is first verified by comparison with centrifuge test results and upper bound plasticity solutions. Both the penetration and the lateral response are demonstrated. The soil strength profile is typical of a soft clay

Fig. 5. Equivalent plastic strain around pipe after vertical penetration (w/D = 0.45).

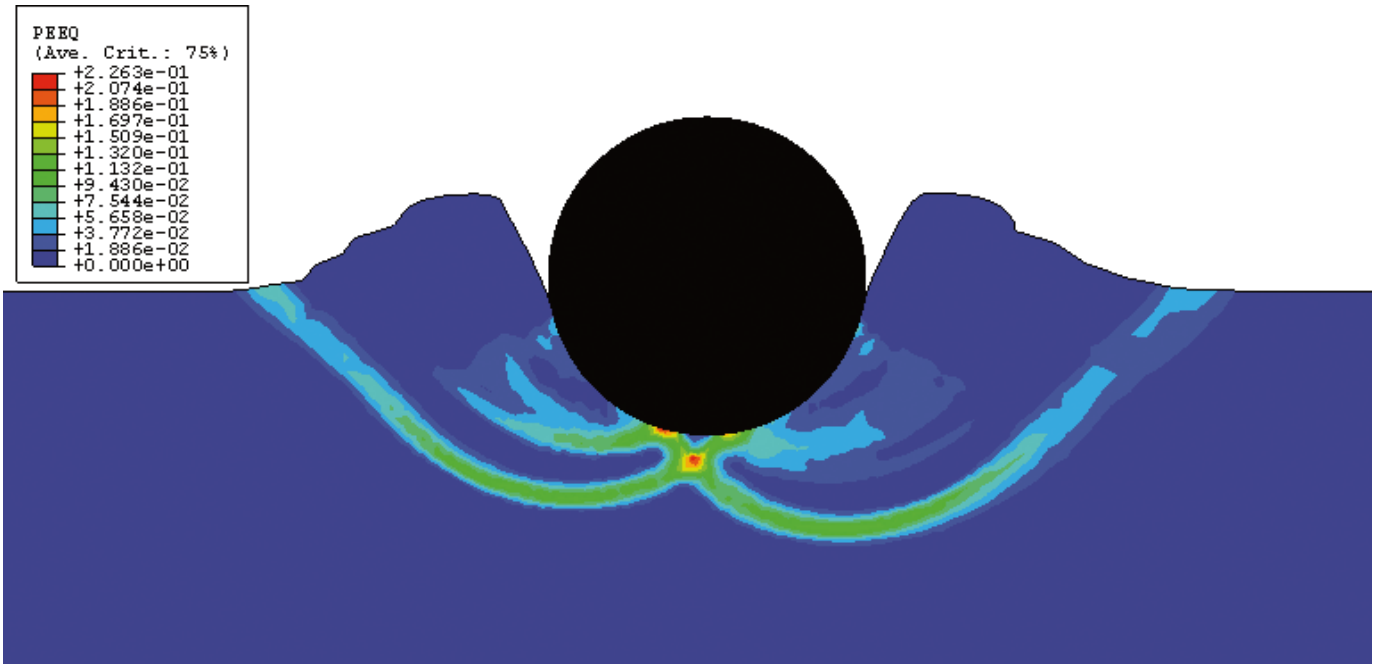

Fig. 6. Penetration resistances based on different mesh density and meshing frequencies: (*a*) fine and coarse mesh used in pipe penetration simulations; (*b*) comparison of penetration resistances (softening rate-dependent soil model).

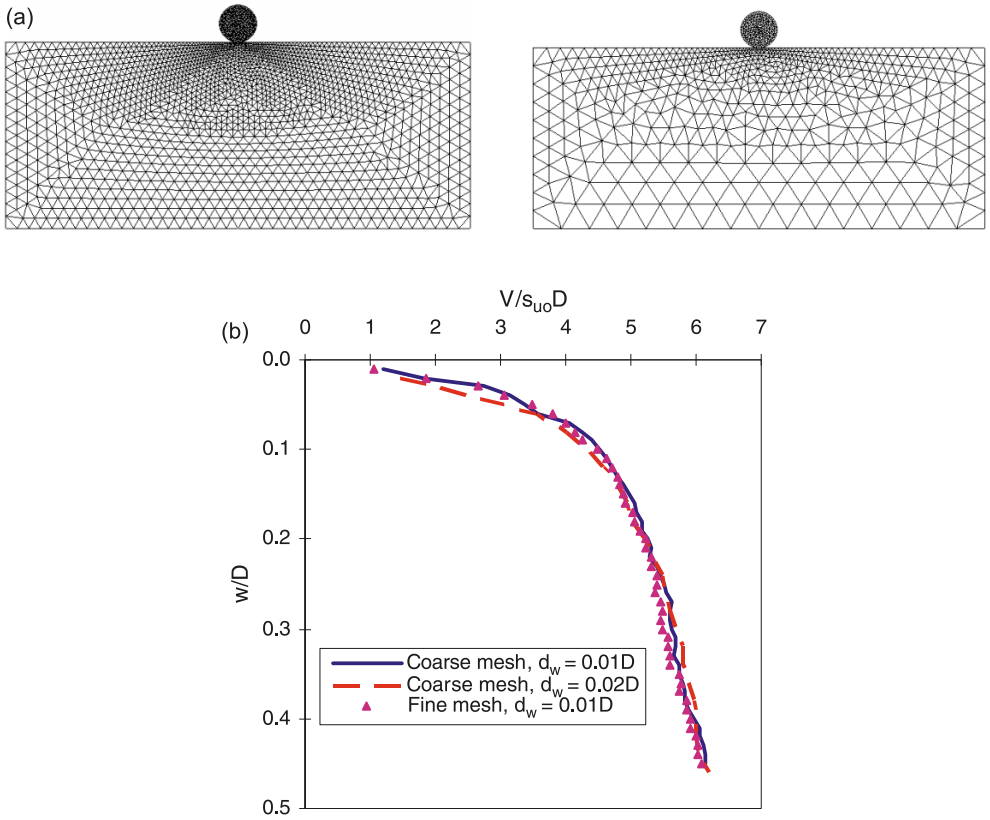

seabed, with a linear original shear strength profile under undrained conditions

$$[4] \qquad s_{u0} = s_{um} + kz$$

where s_{um} is the shear strength at the mudline, k is the strength gradient, and z is the soil depth. The soil is regarded as an elastic – perfectly plastic material obeying the Tresca yield criterion with a strength defined according to eqs. [1] and [4]. Young's modulus of the soil was taken as

Fig. 7. Pipe embedment during lateral displacement (R = 5.26).

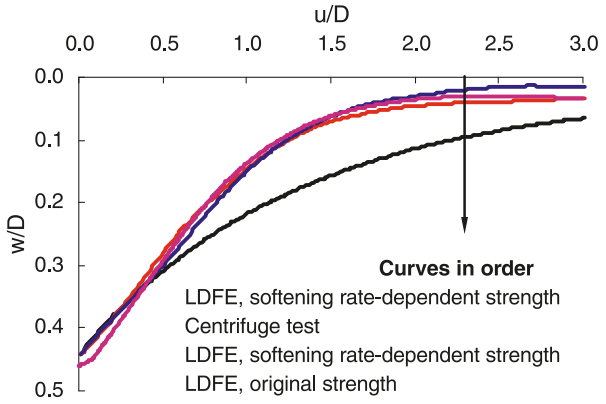

Fig. 8. Lateral load–displacement response (R = 5.26).

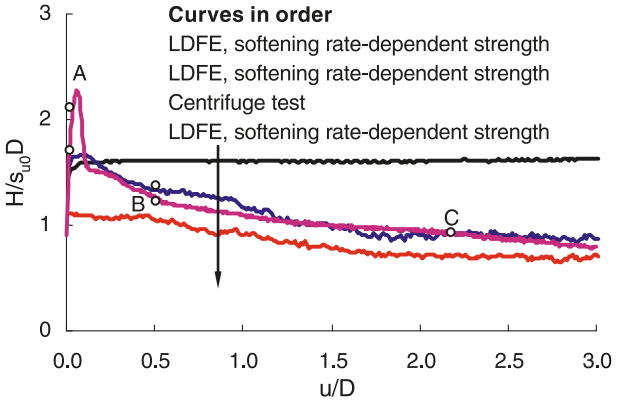

$E = 500s_u$ and Poisson's ratio was taken as 0.49 to approximate undrained conditions.

For simulating the pipe–soil interaction, the pipe and soil surfaces are defined in ABAQUS as master and slave contacts, respectively. The length of contact around the pipe perimeter is permitted to vary as the pipe moves so that the impact of the soil heave and berm on the vertical and lateral resistances is properly captured. The maximum shear stress at the pipe–soil interface is expressed as $\tau_{max} = \alpha s_{um}$, where α denotes the roughness factor of the pipe–soil interface. A value of $\alpha = 0$ corresponds to a fully smooth interface that cannot sustain shear stress. A roughness factor was not directly measured for the centrifuge tests reported by Dingle et al. (2008), and a value of $\alpha = 0.5$ has been adopted in the following LDFE analyses unless stated otherwise. This is similar to, though slightly higher than, the range 0.36–0.43 reported by Chen and Randolph (2007) during continuous penetration of caissons into lightly overconsolidated kaolin clay. During the lateral pipe movement, the suction generated at the rear side of the pipe may produce a tensile resistance bonding the pipe to the soil, but the magnitude of this suction is highly uncertain. The suction is neglected here and the pipeline is assumed to "break away" at its trailing edge; that is, separation occurs at each pipe–soil node once the normal force mobilized between the pipe and the soil at that node falls to zero, with no tensile force permitted.

The parameters adopted in the LDFE analyses are the same as in the Dingle et al. (2008) centrifuge test: prototype pipe diameter D = 0.8 m; submerged unit weight of the clay γ' = 6.5 kN/m^3; and original soil strength determined as s_{um} = 2.3 kPa and k = 3.6 kPa/m through T-bar penetrometer tests. The pipe was penetrated to an embedment $w = 0.45D$, then swept laterally whilst held under a constant vertical operating load of $0.19V_{max}$. For presentation of the results, the vertical and horizontal resistances have been normalized by the original soil strength at the depth of the pipeline invert. In the FE simulations, the bottom and side edges of the soil domain were constrained vertically and horizontally, respectively.

Vertical penetration

Accurate prediction of the pipeline embedment is the greatest challenge during the assessment of lateral behaviour, and embedment is the parameter that most significantly affects the lateral response. Existing methods of estimating pipeline embedment are based on correlations from model tests (e.g., Verley and Lund 1995), theoretical and numerical analyses using limit plasticity (Murff et al. 1989; Randolph and White 2008*a*) or the finite element method (Aubeny et al. 2005; Merifield et al. 2008*a*, 2009). The penetration, w, for a pipeline of diameter D, can be described using the conventional bearing capacity expression, modified for the curved shape of a pipeline

$$[5] \qquad \frac{V}{Ds_{u0}} = N_c + N_b\frac{\gamma' w}{s_{u0}},\ N_b = f_b\frac{A_s}{Dw}$$

where V is the vertical load per unit length, D is the pipeline diameter, s_{u0} is the original shear strength at the pipeline invert, N_c is soil bearing factor, and A_s is the nominal submerged area of the pipe cross section. Based on Archimedes' principle, the buoyancy factor f_b = 1, but a value of f_b = 1.5 is more appropriate due to heave (Randolph and White 2008*b*; Merifield et al. 2009).

The soil bearing factor, N_c, is commonly simplified as a power law expression in terms of the shear strength at the pipeline invert (Aubeny et al. 2005). For the pipe in normally consolidated clays, the penetration resistance can be expressed as

$$[6] \qquad N_c = a\left(\frac{w}{D}\right)^b$$

where a and b are fitted coefficients, depending primarily on the pipe roughness and to a lesser extent on the strength homogeneity parameter, kD/s_{um}. In most studies, the additional vertical resistance related to the soil heave is neglected, and the partially embedded pipeline is assumed to be wished in place.

The vertical load–displacement responses from the LDFE approach and from upper bound (UB) plasticity calculations (Randolph and White 2008*a*) are compared for the case of weightless soil and a smooth pipe–soil interface (Fig. 3*a*). The original soil strength without strain softening and rate-dependence is used in this case. The UB solution slightly exceeds the LDFE penetration resistance by 3%, confirming a previous validation of this numerical procedure (Randolph et al. 2008) and illustrating the insignificant influence of heave on the bearing factor, N_c. In contrast, the soil self-weight has a more significant effect. The soil self-weight

Fig. 9. Instantaneous velocity fields during lateral displacement (R = 5.26): (*a*) point A, (*b*) point B, and (*c*) point C in Fig. 8.

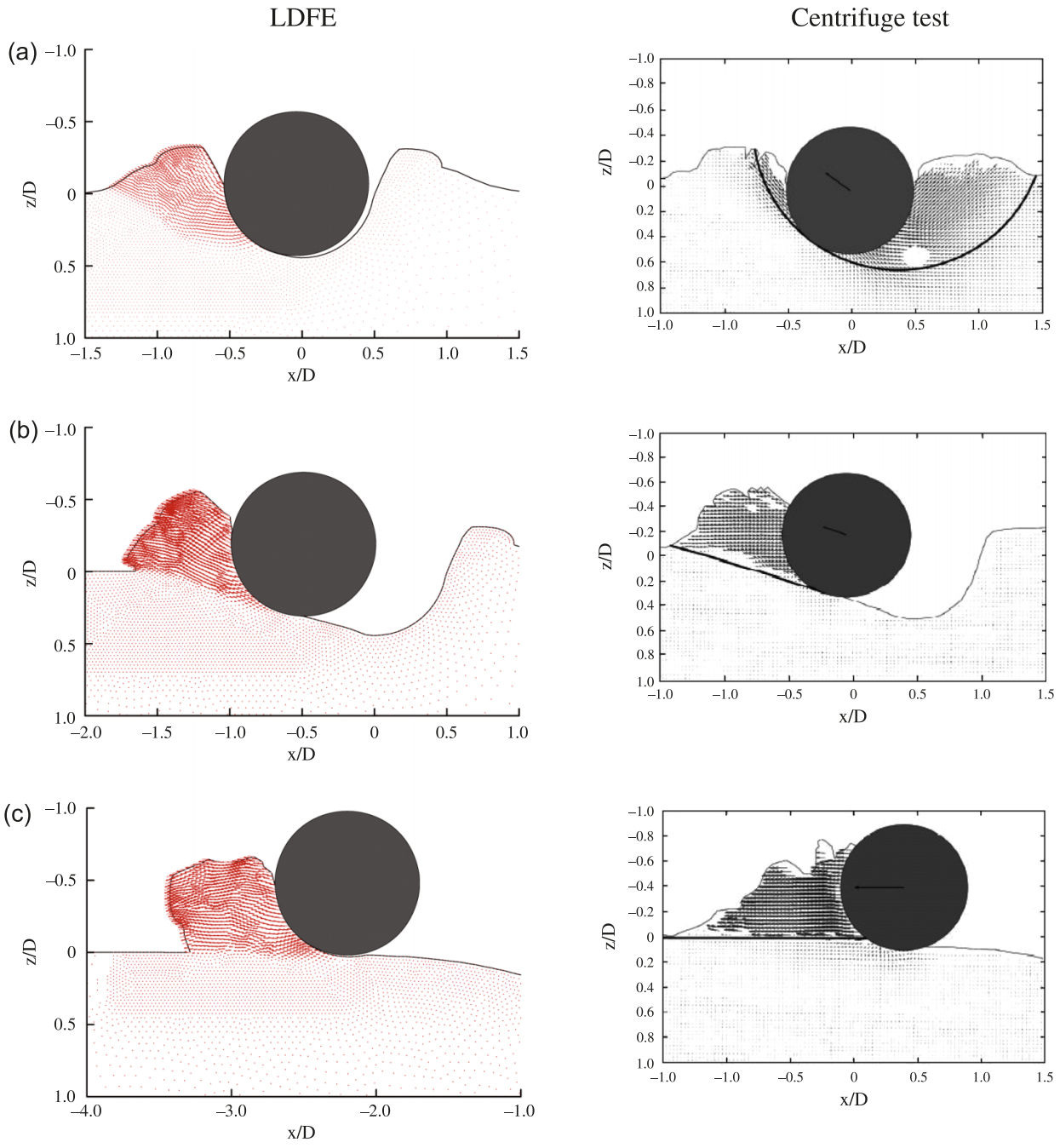

leads to the buoyancy term in eq. [5], quantified through N_b, which reflects the potential energy needed to lift the soil displaced during an increment of penetration to the top of the pre-existing heave profile. By including soil weight in the LDFE analysis, the additional component of penetration resistance due to buoyancy given in eq. [5] can be assessed directly. For a smooth pipe, the additional resistance due to the soil weight is calculated as the difference in $V/s_{u0}D$ for the weighty and weightless cases and can be used to derive the buoyancy factor, f_b, directly. As shown in Fig. 3*b*, the back-calculated profile of f_b is close to 1.5, which is the value recommended by Merifield et al. (2009). This buoyancy exceeds the value of unity predicted by Archimedes' principle due to the additional elevation of the heave.

The effect of the pipe–soil roughness is also indicated in Fig. 3*a*. The penetration resistance for the fully rough case (α = 1) is 14% greater than for the fully smooth case (α = 0) at an embedment of w/D = 0.5. This difference may appear small but is significant when considered instead as the effect of roughness on pipe embedment under a given load. For a load of $V/s_{u0}D$ = 5, the penetration for a smooth interface is 0.44D, but only 0.24D for a rough interface – a factor of 2 difference.

When the LDFE results and the centrifuge test data are

Fig. 10. Effect of pipe weight on the trajectory during lateral displacement.

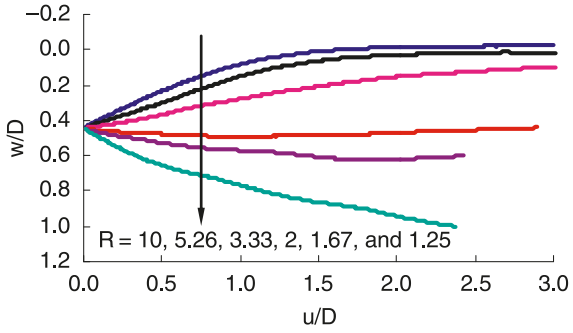

compared (Fig. 3*b*), it is found that the resistance based on the nonsoftening rate-independent shear strength soil model is significantly lower than that measured in the centrifuge test. Two possible reasons for this are unreliable quantification of the soil strength at shallow depths in the experimental data and the dependence of the soil strength on the loading rate and strain softening. The linearly fitted strength profile, $s_{u0} = (2.3 + 3.6z)$ kPa, may not be strictly accurate for shallow depths. Also, some softening is inevitable during penetration of the pipe. The strength measured by the T-bar test relates to a fully flow-round mechanism, in which there is a significant degree of soil remoulding. In contrast, the initial shallow penetration of a pipeline involves less remoulding, and so an enhanced strength is relevant. To capture both the softening and rate-dependent behaviour, a further LDFE simulation was conducted using the strength model described in eq. [1] with constitutive parameters $S_t = 3.2$, $\mu = 0.1$, and $\xi_{95} = 10$ as reported by Zhou et al. (2008). As reported by Dingle et al. (2008), the model pipe was penetrated with a velocity $v_p = 0.015D$/s. With these parameters, good agreement with the centrifuge test data is achieved.

The instantaneous velocity fields at $w/D = 0.07$, 0.25, and 0.35 are shown in Fig. 4 for the LDFE analysis incorporating strain rate and softening effects. The velocity distributions predicted by the LDFE analysis match well the velocity results from the images captured in the centrifuge test. In particular, it is notable that the velocity distributions are no longer symmetric about the pipe centreline when the embedment ratio increases to 0.25 and 0.35. This is due to the softening of the shear zone after the full strength has been mobilized. In both the centrifuge test and the LDFE, the shear zones do not move continuously downwards with the penetrating pipe. Instead, distinct shear zones form on alternate sides of the pipe at intervals (Dingle et al. 2008). This intermittent shedding of shear zones results from the failure mechanism becoming concentrated in the softened soil. This zone softens further until the distorted geometry of the failure mechanism overcomes the beneficial influence of the softened soil. At this point a new shear zone forms ahead of the pipe. The same behaviour has been observed in an LDFE analysis of a deeply buried T-bar penetrometer in strain-softening soil (Zhou and Randolph 2007).

If the soil mesh in FE analyses is strictly symmetric about the pipe centreline, the intermittent shear band shedding may not take place. A free meshing strategy is used here to generate a nonsymmetric mesh, which permits asymmetric mechanisms to develop in the same way as from natural nonhomogeneity in soil. The deformed mesh and contours of equivalent plastic strain increment at $w/D = 0.45$ are shown in Fig. 5. The intermittent shear bands can be observed clearly. The LDFE results are mesh-independent, provided a nonsymmetric mesh is used initially. This asymmetry in the mesh is required to create asymmetry in the behaviour, allowing the optimal failure mechanism to be mobilized, because this involves intermittent shear band generation. In Fig. 6, the penetration resistances based on a fine mesh and a coarse mesh are compared. When the coarse mesh was used, the pipe displacement in each incremental step was taken as either $dw = 0.01D$ (as used for the fine mesh) or $0.02D$. The close agreement in the computed penetration responses indicates that the results are essentially independent of the mesh density and remeshing frequency. These comparisons of the internal deformation and the mobilized resistance provide detailed validation of the ABAQUS-based LDFE approach. These results also indicate that a softening rate–dependent model is required to capture the detailed deformation patterns during pipe penetration into clay.

Large-amplitude lateral displacement

In the centrifuge test reported by Dingle et al. (2008), the overpenetration ratio was $R = 1/0.19 = 5.26$ and the lateral pipe velocity was $0.05D$/s at model scale. The pipe was displaced horizontally while the vertical load remained constant and the pipe was free to move upwards or downwards. Three LDFE analyses were carried out, based on the original strength profile and the following soil models: (*i*) without softening or rate dependency, (*ii*) with softening but with rate-independent strength, and (*iii*) with softening and rate-dependent strength. The constitutive parameters relating strain softening and rate-dependence are the same as in the vertical penetration simulation except that $v_p = 0.05D$/s to match the lateral displacement test stage.

Figure 7 shows the trajectory of the pipe invert, where u represents the pipe lateral displacement. In the centrifuge, the pipe moved upwards towards the soil surface until reaching a steady elevation of $\sim 0.03D$ below the original soil surface. The pipe lateral displacement at which this steady elevation was reached was about $2.2D$. All LDFE analyses reproduced the upwards pipe movement; but when the soil strength is characterized by the original profile, the trajectory of the pipe is flatter than in the test. For the softening model without rate-dependence, the steady embedment is slightly shallower than the experimental result. When the rate-dependent softening model is employed in the numerical analysis, the evolution of the pipe embedment is very similar to the test. The rate dependence increases the rate of plastic work in the zone of intense shearing, encouraging the pipe to move upwards more to reduce the size of the deforming region.

Figure 8 compares the lateral load–displacement response during each of the three LDFE simulations with the centrifuge test data, where H denotes the mobilized lateral resistance. In the centrifuge, the pipe resistance mobilized a brittle peak value after the pipe invert had moved only $0.06D$ laterally and then dropped sharply due to the loss of contact at the rear of the pipe. After this brittle breakout, the normalized resistance reduces slowly as the pipe sweeps lat-

Fig. 11. Soil flow mechanisms for a heavy pipe (R = 1.25).

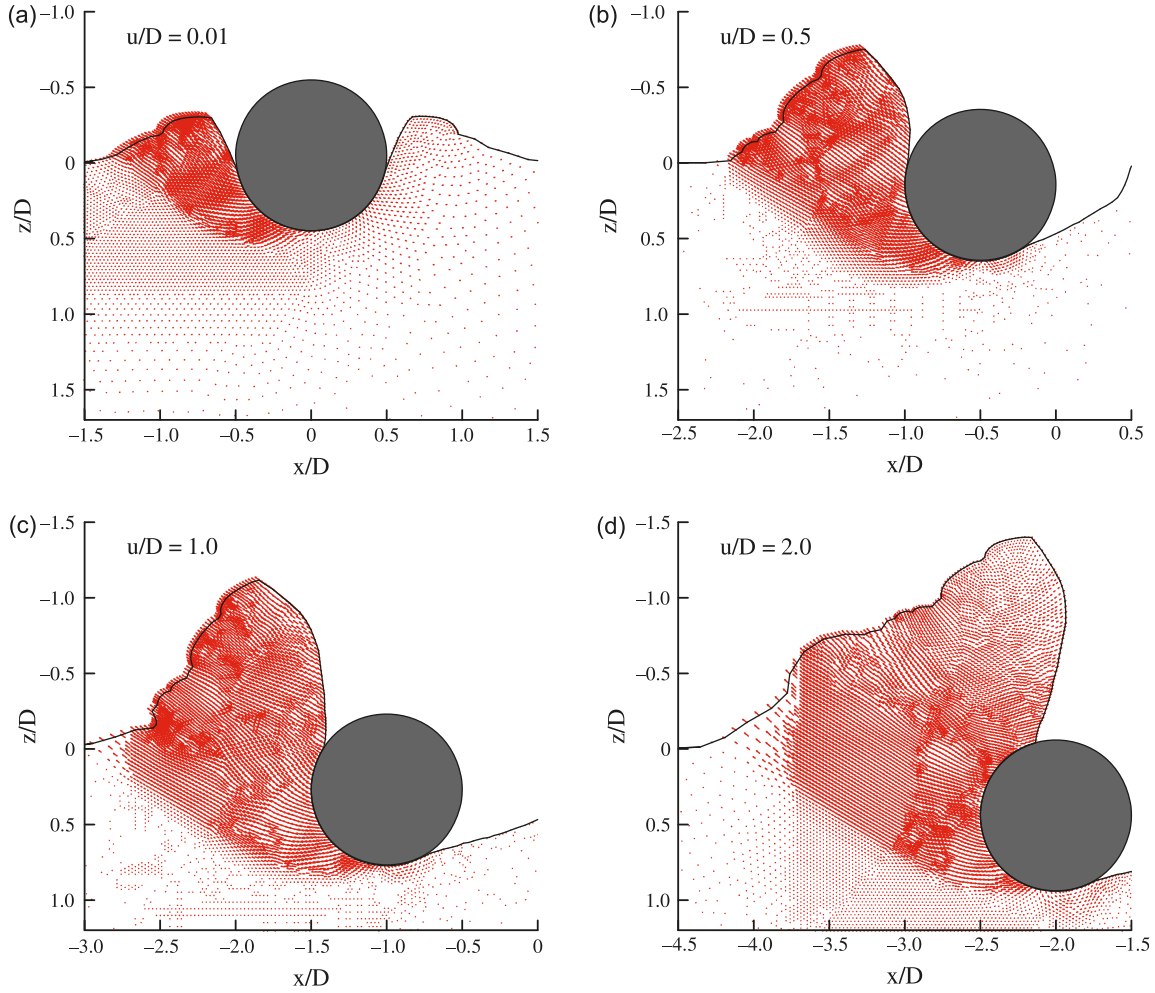

erally. As mentioned previously, the pipe–soil interface used in these numerical simulations does not permit tensile resistance at the rear of the pipe, so the LDFE analyses do not capture the brief brittle peak evident in the centrifuge model.

If the rate-dependence and softening of strength are not considered in the LDFE simulation, the normalized lateral resistance, $H/s_{u0}D$, remains almost constant after reaching the maximum value, which is not in accordance with the centrifuge observations. The horizontal resistance based on the softening but rate-independent model is slightly lower than the experimental data. Similar to the penetration behaviour in the above section, the LDFE analysis based on softening and rate-dependent strength provides the closest agreement between the numerical and experimental results.

The comparison shown in Figs. 7 and 8 indicates that a rate-dependent strain-softening model for soil strength gives a more realistic response in terms of both the pipe trajectory and the lateral resistance, compared with simpler models without both effects.

Three positions labelled A–C in Fig. 8 have been selected to show the soil flow mechanisms during the lateral displacement process (Fig. 9). At the initial stage (point A), there is no breakaway between the soil and rear face of the pipeline in the centrifuge test due to the tensile resistance sustained through negative excess pore pressure. The displacement vectors from PIV analysis indicate that a double-sided failure mode is beginning to develop. However, no distinct shear zones form behind the pipe and the maximum resistance is instead governed by the tension that is mobilized prior to separation.

In contrast, the soil separates from the rear face of the pipeline in the LDFE analyses and the soil heave formed during the vertical penetration stage is wholly located within the zone of failing soil. At point B, which corresponds to a lateral displacement of u/D = 0.5, the soil berm slides upwards along a failure surface that passes through the toe of the soil berm, and the soil displacements under the failure surface are negligible. The agreement between the LDFE and centrifuge results is remarkable. The pipe rises gradually to a steady elevation at point C, where the failure mechanism is essentially sliding along the base of the soil berm. The berm-sliding mechanism governs the residual resistance from point B to point C. In Fig. 9, the velocity fields from the LDFE analysis and centrifuge test agree closely, confirming the general mechanisms of behaviour. It is notable that the soil berm in the centrifuge test has a sloping face, suggesting a greater loss of strength compared with the near-vertical cliff at the front of the LDFE berm. The lower

residual resistance within the centrifuge test is further evidence that greater softening occurs within the soil berm and at the base.

Effect of pipe weight on lateral response

Pipe trajectory

The previous analyses provide a good representation of pipe–soil interaction during large-amplitude lateral displacement. The general form of the lateral response comprises a peak in resistance as the pipe breaks out, followed by a relatively constant residual resistance. However, this form of response is not appropriate for all pipelines embedded on clay. The following set of analyses explore the trajectory and load–displacement response for pipes of different normalized operating weights, $V/s_{u0}D$, penetrated to the same initial conditions as the centrifuge test. The purpose of these analyses is to show that the pipe weight, normalized by the local soil strength, affects the entire shape of the large-amplitude lateral response, not just the magnitude of the resistance.

A suite of LDFE analyses were undertaken, varying the initial overpenetration ratio, $R = 1.25 \sim 10$, based on $V_{max}/Ds_{u0} = 6.2$ to give the initial penetration of $w/D = 0.45$. All other parameters were the same as in the optimal back-analysis of the centrifuge model test. The resulting pipe invert trajectories are shown in Fig. 10.

For values of overpenetration ratio, $R > 2$, the pipes rise to reach a steady elevation, which is very close to the soil surface. For $R = 10$, the pipe rises even above the original surface elevation. In contrast, for a value of $R < 2$, the pipes move downward to a deeper elevation. The terms "light" and "heavy" pipes have been used to capture this distinction between upward and downward pipe movement during lateral breakout (Bruton et al. 2008).

The centrifuge test is an example of a "light" pipe response, which involves the soil flow mechanisms shown in Fig. 9, ultimately reaching a near steady-state resistance associated with sliding of a soil berm. Contrasting behaviour is observed for the "heavy" pipes with $R \leq 2$. The downward pipe movement quickly leads to the growth of a high soil berm ahead of the pipe, which tends to fall over the crown of the pipe (Fig. 11). While the soil flow mechanism of a light pipe is characterized by the berm-sliding mode, the heavy pipe mobilizes a deep shearing zone that expands with continuing lateral movement.

Lateral load–displacement response

The different lateral load–displacement responses for the various values of R are shown in Fig. 12, in two normalized forms: "friction factor", H/V (Fig. 12*a*), and $H/s_{u0}D$ (Fig. 12*b*), where s_{u0} is updated to the strength at the current elevation based on the initial s_{u0} profile. At first glance, both normalizations appear useful. Initially, similar values of $H/s_{u0}D$ are evident whilst H/V varies by an order of magnitude. After 1 diameter of lateral displacement, H/V ranges only from 0.7 to 0.9, but the responses cross and diverge, with the friction factor of the heaviest pipe continuing to rise beyond $H/V = 1$ at $u/D = 2.0$, whilst the responses for the lighter pipes approach steady, but lower values. For the alternative normalization, the range is $0.6 < H/s_{u0}D < 3.7$ at the end of the lateral sweep. Neither normalization consistently unifies the different cases.

Fig. 12. Effect of pipe weight on the horizontal resistance during lateral displacement. (*a*) Friction factor, H/V; (*b*) normalized horizontal resistance, $H/s_{u0}D$.

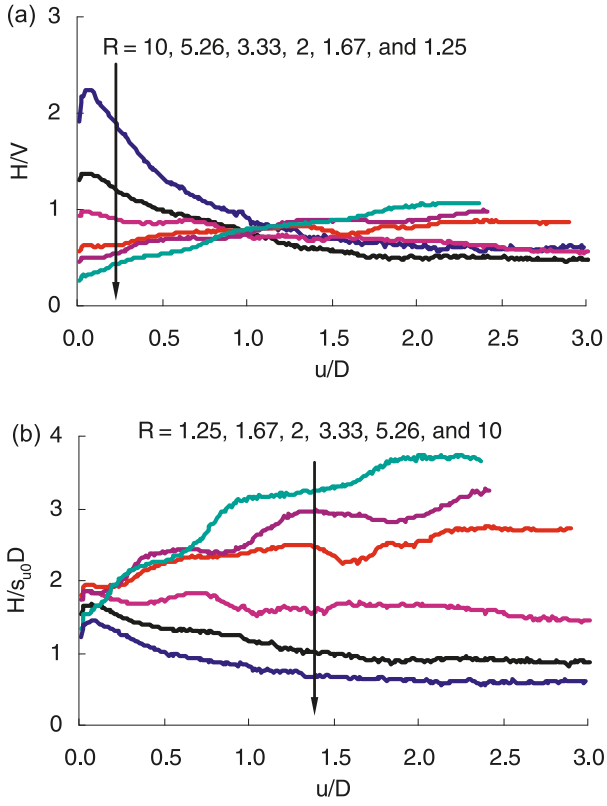

The differing forms of lateral load response are linked to the trajectory of the pipe. For all values of the overpenetration ratio, the initial breakout resistance is approximately the same, as the pipe movement is close to horizontal and the embedment is the same. For this failure mechanism, the vertical load has minimal influence on the work input. However, as the "light" pipes move upwards, the failure mechanism reduces in size and the soil carried ahead of the pipe within the berm softens. This leads to reduction in the resistance H (which exceeds the reduction in s_{u0} associated with the reducing embedment), and so $H/s_{u0}D$ decays slightly with displacement.

In contrast, the downward movement of the "heavy" pipes leads to an increase in resistance (beyond that associated with the rising s_{u0}) as the failure mechanism grows. The resulting profiles of resistance show a continuous rise in $H/s_{u0}D$. Although the analyses for the heaviest pipes were halted at a displacement of $u/D = 2.4$, this trend of rising normalized resistance is anticipated to continue until a deep flow-round mechanism is mobilized.

Given these differing mechanisms for "light" and "heavy" pipes, it is obvious that the friction factor normalization does not capture the underlying mechanism. It is important to recognise that the underlying soil flow mechanisms are entirely different for the light and heavy pipes — as evident in the contrast between the berm-sliding shown in Fig. 9*c* and the deep ploughing in Fig. 11*d*. An al-

Fig. 13. Comparison of upper bound yield envelope and ultimate loads in LDFE analysis.

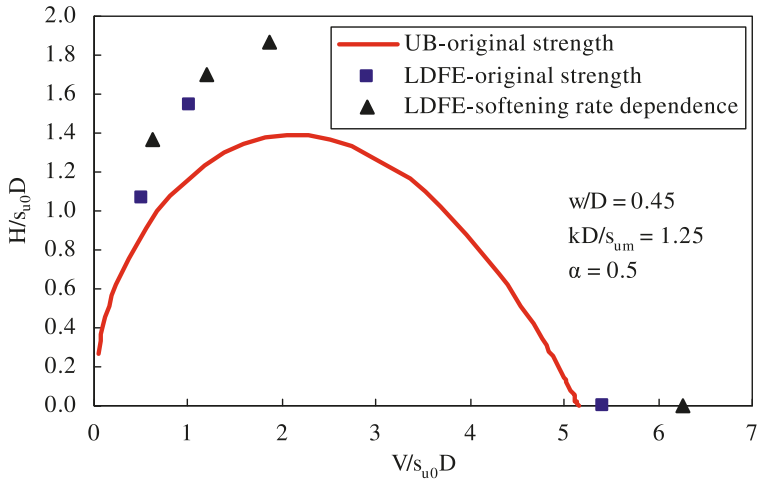

ternative approach that provides a more consistent normalization of the large-amplitude lateral response is described later in this paper.

Comparison with theoretical yield envelopes

Yield envelopes defining the combinations of vertical and horizontal load at failure can be used to explore the contrasting behaviour between "light" and "heavy" pipes. A yield envelope from the upper bound plasticity solution presented by Randolph and White (2008*a*) is compared with the maximum loads from the LDFE analyses in Fig. 13. The yield envelope shown corresponds to the initial embedment of $w/D = 0.45$. In upper bound solutions, the pre-embedded pipeline was wished into place in weightless soil and a generalized version of the Martin mechanism (Martin and Randolph 2006) was devised.

The LDFE results are shown in Fig. 13 for both the ideal and softening rate–dependent soil models, but only the light pipes that showed a distinct peak in resistance during breakout are included. The loads from the LDFE approach are all located outside the yield envelope from the limit analyses. Also highlighted on this figure are the vertical loads during the initial penetration stage, which exceed the plasticity solution due to the influence of heave and buoyancy. The breakout lateral resistance from the LDFE approach is also higher than the UB envelope – by almost 30% in some cases. These observations show that soil heave and buoyancy have an influence on lateral breakout resistance in addition to vertical embedment.

The direction of pipe movement at failure, dw/du, can also be estimated from the yield envelopes, using the associated flow rule (or normality). (A normal to the yield envelope indicates the direction of plastic movement at failure, using conjugate axes of displacement — this link is known as a flow rule in plasticity analysis.) Fig. 14 compares the theoretical flow rule from the yield envelope with the LDFE results. Close agreement is evident, although the LDFE results correspond to a flatter trajectory. In both cases, the upward inclination of the light pipe movement increases with the overpenetration ratio, and the downward inclination of the heavy pipe movement increases with the decrease of the overpenetration ratio. The overpenetration ratio that distinguishes "light" and "heavy" pipes is $V_{op}/V_{max} = 0.42$ ($R = 2.38$) from the upper bound solutions, which corresponds to $V_{op}/s_{u0}D = 2.6$ for $w/D = 0.45$. This matches the LDFE analyses in which values of $R = 3.33$ and 2 show "light" and "heavy" behaviour, respectively.

Alternative interpretation of large-amplitude lateral response

Once the pipe breaks out and the geometry of the soil surface is disturbed, the theoretical yield envelopes are no longer appropriate. The responses of both the "light" and "heavy" pipes are dominated by the zone of soil ahead of the pipe — a remoulded berm for a "light" pipe and a wall of intact soil for a "heavy" pipe. The following interpretation of the LDFE results provides a technique for capturing both forms of response, which is more accurate and representative of the governing mechanisms than the conventional "friction factor" approach.

The variation in normalized lateral resistance, $H/s_{u0}D$, with embedment for all six analyses is shown in Fig. 15*a*. For "heavy" pipes, the normalized resistance is enhanced by downward movement due to the increased passive resistance arising from the wall of soil ahead of the pipe. In contrast, the normalized resistance of a light pipe decreases as the pipe rises. However, the flow mechanisms for both "light" and "heavy" pipes depend strongly on the development of the soil berm or wall ahead of the pipe (Figs. 9, 11). There is no unique relationship between $H/s_{u0}D$ and w/D for all "heavy" and "light" pipes in Fig. 15*a*. This is because the additional component of embedment due to the soil berm is not captured by w/D. Instead, the concept of an effective embedment ratio, w'/D, can be used, where w' represents a modified embedment accounting for the height of the berm or wall of soil ahead of the pipe.

The basis of this effective embedment concept is as follows (see Fig. 16):

(1) The berm is idealized as a rectangular block with an aspect ratio (width/height) of η. The idealized berm height can be calculated from the berm area, A_{berm}, as $h_{berm} = \sqrt{A_{berm}/\eta}$.

(2) The soil within the berm is heavily but not fully re-

Fig. 14. Inclination of displacement paths at lateral breakout from upper bound solutions and LDFE analysis (at $u/D \approx 0.05$).

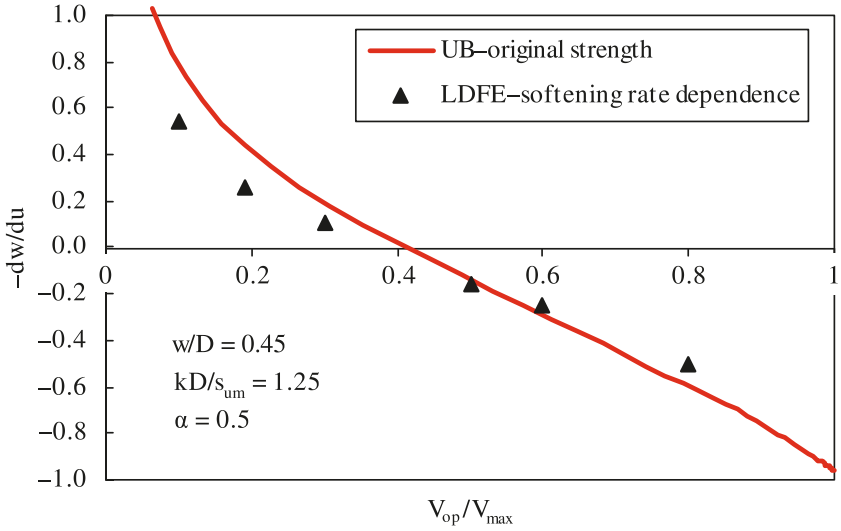

Fig. 15. Variation of lateral resistance with embedment and effective embedment. (*a*) Normalized embedment, w/D; (*b*) adjustmed normalized embedment, w'/D.

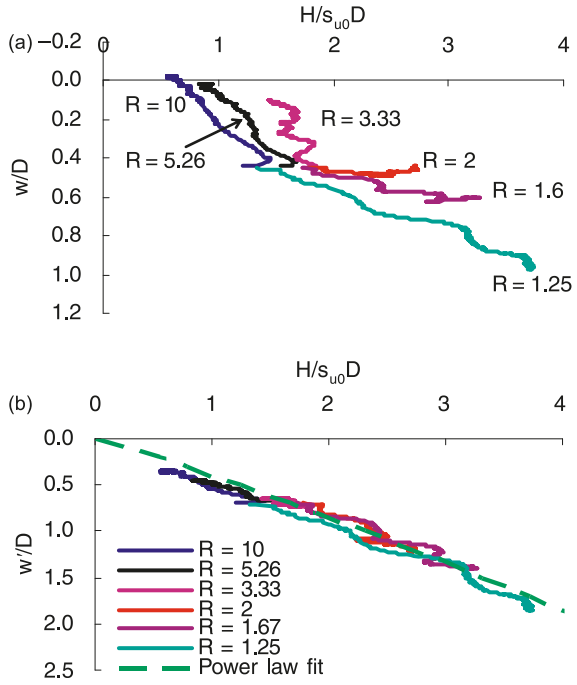

moulded, so the operative strength is assumed to be reduced by a factor $S_{t,berm} = \lambda S_t$, where λ represents the degree of softening within the berm compared with full softening to the remoulded strength. To account for this reduced strength acting within the berm, the additional embedment created by the berm is factored down by $S_{t,berm}$, thus equalling $h'_{berm} = h_{berm}/S_{t,berm} = h_{berm}/(\lambda S_t)$.

(3) This logic leads to the following expression for effective embedment ratio:

$$[7] \qquad \frac{w'}{D} = \frac{w}{D} + \frac{h'_{berm}}{D} = \frac{w}{D} + \frac{1}{S_{t,\,berm} D}\sqrt{\frac{A_{berm}}{\eta}}$$

The berm area can be calculated directly from the coordinates of the soil surface nodes that are above the original soil surface or can be assessed from the area swept by the pipe. The embedment in Fig. 15*a* is then converted to the effective embedment by eq. [7]. Figure 15*b* shows the variation in normalized resistance with effective embedment for all six pipe simulations, where values of $\eta = 1.0$ and $\lambda = 0.5$ (so that $S_{t,berm} = 0.5\ S_t$) have been adopted by observing the berm shape and reduced soil strength within the berm indicated by the LDFE.

When expressed in this format, the data for all cases ($R = 1.25 \sim 10$) fall in a narrow band. Also shown in Fig. 15*b* is the following power law fit, which is similar to eq. [6]:

$$[8] \qquad \frac{H}{s_{u0}D} = a\left(\frac{w'}{D}\right)^b$$

where $a = 2.3$ and $b = 0.9$. The close agreement between all FE results suggests that the lateral resistance is relatively unaffected by the precise trajectory of the pipe, over the range encountered in the above simulations. The lateral resistance can be considered a function only of the effective embedment. The evolution of this embedment depends on the pipe weight relative to the local soil strength. "Light" pipes rise to a steady embedment very close to the soil surface, whereas "heavy" pipes sink to a significant embedment exceeding one diameter.

Conclusions

In the design of on-bottom pipelines, the lateral pipe–soil resistance must be estimated to assess lateral buckling and estimate the passive restraint during a submarine slide impact. Previous theoretical studies have focused on the lateral response at small pipe displacements. These studies have generally ignored the effects of both soil heave during initial penetration and distortion of the seabed surface during large movements. In this paper, the full process of vertical penetration followed by large-amplitude lateral displacement has been investigated using an LDFE approach with mesh regeneration. A simple softening rate–dependent soil strength model has been incorporated into the LDFE analysis to rep-

Fig. 16. Basis for assessing effective embedment. A'_{berm}, reduced berm area allowing for soil softening.

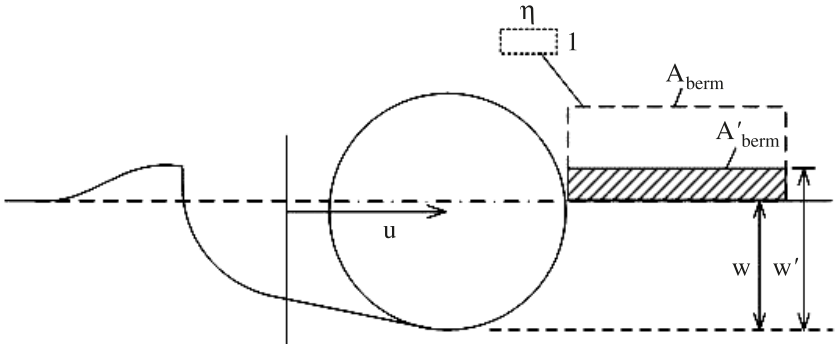

licate the intermittent shear band shedding observed in model tests and to capture the detailed soil flow patterns observed in experiments. The LDFE approach has been verified by comparison with upper bound plasticity analysis and a centrifuge test of pipe–soil interaction in kaolin clay. Excellent agreement is achieved in terms of both the instantaneous soil flow mechanisms and also the lateral resistance and pipe trajectory.

A parametric study has been conducted to explore the influence of pipe weight on the lateral resistance and trajectory. Two distinct modes of large-amplitude lateral response are evident, corresponding to "light" and "heavy" pipes — which can be distinguished by the pipe weight relative to the local soil strength or simply the overpenetration ratio, R. The failure mechanism, pipe trajectory, and soil berm evolution observed for "light" pipes are entirely different from the "heavy" ones. "Light" pipes rise and push a berm of soil across the soil surface. "Heavy" pipes dive and shear both intact soil and a remoulded berm.

During initial lateral breakout, the observed resistance is poorly represented by a "friction factor" definition and is better captured by a failure envelope approach. After significant lateral movement, the apparent friction factors for both "light" and "heavy" pipes lie in a narrow range, despite different mechanisms, with a sliding surface berm for "light" pipes and deep ploughing for "heavy" pipes. The entire response of both "light" and "heavy" pipes, from breakout to large displacement, may be captured by considering the deformed surface geometry ahead of the pipe. The concept of an effective embedment has been proposed to account for the height of the berm or wall of soil ahead of the pipe. This concept unifies the response for a range of values of pipe weight. For an overpenetration ratio in the range of $R = 1.25 \sim 10$, the normalized lateral resistance is a power law function of the effective embedment and is unaffected by the trajectory of the pipe.

Acknowledgements

The work described here forms part of the activities of the Centre for Offshore Foundation Systems (COFS), established under the Australian Research Council's Research Centres Program and now supported under grant FF0561473 from the Australian Research Council (ARC) and Centre of Excellence funding from the State Government of Western Australia. This research forms part of the activity for ARC research grant LX0664864 and contributes to joint industry project M395 supported by the Minerals and Energy Institute of Western Australia (MERIWA) and six industry sponsors (BP, BHP Billiton, Chevron, Petrobras, Shell, and Woodside).

References

Aubeny, C.P., Shi, H., and Murff, J.D. 2005. Collapse load for cylinder embedded in trench in cohesive soil. International Journal of Geomechanics, **5**(4): 320–325. doi:10.1061/(ASCE)1532-3641(2005)5:4(320).

Bruton, D.A.S., White, D.J., Carr, M., and Cheuk, C.Y. 2008. Pipe-soil interaction during lateral buckling and pipeline walking – the Safebuck JIP. *In* Proceedings of Offshore Technology Conference, Houston, Tex., 5–8 May 2008. Offshore Technology Conference, Richardson, Tex. OTC 19589.

Carter, J.P., and Balaam, N.P. 1995. AFENA user manual. Version 5.0 [computer program]. Geotechnical Research Centre, The University of Sydney, Sydney, Australia.

Chen, W., and Randolph, M.F. 2007. Radial stress changes and axial capacity for suction caissons in soft clay. Géotechnique, **57**(6): 499–511. doi:10.1680/geot.2007.57.6.499.

Cheuk, C.Y., White, D.J., and Dingle, H.R.C. 2008. Upper bound plasticity analysis of a partially-embedded pipe under combined vertical and horizontal loading. Soils and Foundations, **48**(1): 133–140.

Dingle, H.R.C., White, D.J., and Gaudin, C. 2008. Mechanisms of pipe embedment and lateral breakout on soft clay. Canadian Geotechnical Journal, **45**(5): 636–652. doi:10.1139/T08-009.

Einav, I., and Randolph, M.F. 2005. Combining upper bound and strain path methods for evaluating penetration resistance. International Journal for Numerical Methods in Engineering, **63**(14): 1991–2016. doi:10.1002/nme.1350.

HKS. 2006. ABAQUS users' manual. Version 6.5 [computer program]. Hibbitt, Karlsson and Sorensen, Inc., Pawtucket, R.I.

Hu, Y., and Randolph, M.F. 1998. A practical numerical approach for large deformation problem in soil. International Journal for Numerical and Analytical Methods in Geomechanics, **22**(5): 327–350. doi:10.1002/(SICI)1096-9853(199805)22:5<327::AID-NAG920>3.0.CO;2-X.

Konuk, I., and Yu, S. 2007. Continuum FE modelling of lateral buckling: study of soil effects. *In* Proceedings of the 26th International Conference on Offshore Mechanics and Arctic Engineering, San Diego, Calif., 10–15 June 2007. American Society of Mechanical Engineers, Houston, Tex. Paper No. OMAE2007-29376.

Martin, C.M., and Randolph, M.F. 2006. Upper-bound analysis of

lateral pile capacity in cohesive soil. Géotechnique, **56**(2): 141–145. doi:10.1680/geot.2006.56.2.141.

Merifield, R., White, D.J., and Randolph, M.F. 2008*a*. The ultimate undrained resistance of partially embedded pipelines. Géotechnique, **58**(6): 461–470. doi:10.1680/geot.2008.58.6.461.

Merifield, R.S., White, D.J., and Randolph, M.F. 2008*b*. The effect of pipe–soil interface conditions on the undrained breakout resistance of partially-embedded pipelines. *In* Proceedings of the 12th International Conference of International Association for Computer Methods and Advances in Geomechanics, Goa, India, 1–6 October 2008. pp. 4249–4256.

Merifield, R.S., White, D.J., and Randolph, M.F. 2009. Effect of surface heave on response of partially embedded pipelines on clay. Journal of Geotechnical and Geoenvironmental Engineering, **135**(6): 819–829. doi:10.1061/(ASCE)GT.1943-5606.0000070.

Murff, J.D., Wagner, D.A., and Randolph, M.F. 1989. Pipe penetration in cohesive soil. Géotechnique, **39**(2): 213–229. doi:10.1680/geot.1989.39.2.213.

Randolph, M.F., and White, D.J. 2008*a*. Upper-bound yield envelopes for pipelines at shallow embedment in clay. Géotechnique, **58**(4): 297–301. doi:10.1680/geot.2008.58.4.297.

Randolph, M.F., and White, D.J. 2008*b*. Pipeline embedment in deep water: process and quantitative assessment. *In* Proceedings of the Offshore Technology Conference, Houston, Tex., 5–8 May 2008. Curran Associates, Inc., Red Hook, N.Y. Paper OTC19128.

Randolph, M.F., Wang, D., Hossain, M.S., Zhou, H., and Hu, Y. 2008. Large deformation finite element analysis for offshore applications. *In* Proceedings of the12th International Conference of International Association for Computer Methods and Advances in Geomechanics, Goa, India, 1–6 October 2008. pp. 3307–3318.

Swanson, R.C., and Jones, W.T. 1982. Mudslide effects on offshore pipelines. Transportation Engineering Journal, **108**(6): 585–600.

Verley, R., and Lund, K.M. 1995. A soil resistance model for pipelines placed on clay soils. *In* Proceedings of the 14th International Conference on Offshore Mechanics and Arctic Engineering, Copenhagen, Denmark, 18–22 June 1995. American Society of Mechanical Engineers (ASME), New York. Vol. 5, pp. 225–232.

Wang, D., Hu, Y., and Jin, X. 2006. Two-dimensional large deformation finite element analysis for the pulling-up of plate anchor. China Ocean Engineering, **20**(2): 269–279.

Wang, D., Hu, Y., and Randolph, M.F. 2010. Three-dimensional large deformation finite element analysis of plate anchors in uniform clay. Journal of Geotechnical and Geoenvironmental Engineering, **136**(2): 355–365. doi:10.1061/(ASCE)GT.1943-5606.0000210.

White, D.J., Take, W.A., and Bolton, M.D. 2003. Soil deformation measurement using particle image velocimetry (PIV) and photogrammetry. Géotechnique, **53**(7): 619–631.

Zhou, H., and Randolph, M.F. 2007. Computational techniques and shear band development for cylindrical and spherical penetrometers in strain-softening clay. International Journal of Geomechanics, **7**(4): 287–295. doi:10.1061/(ASCE)1532-3641(2007)7:4(287).

Zhou, H., and Randolph, M.F. 2010. Numerical investigations into cycling of full-flow penetrometers in soft clay. Géotechnique, **59**(10): 801–812.

Zhou, H. White. D.J., and Randolph, M.F. 2008. Physical and numerical simulation of shallow penetration of a cylindrical object into soft clay. *In* Proceedings of the ASCE GeoCongress 2008, New Orleans, La., 9–12 March 2008. American Society of Civil Engineers, Reston, Va. pp. 108–117.

Zienkiewicz, O.C., and Zhu, J.Z. 1992. The superconvergent patch recovery and a posteriori error estimates. Part 1: The recovery technique. International Journal for Numerical Methods in Engineering, **33**(7): 1331–1364. doi:10.1002/nme.1620330702.